ACCEPTED VERSION

S. Dini, B.J. Binder, J.E.F. Green
Understanding interactions between populations: individual based modelling and quantification using pair correlation functions

Final publication at http://dx.doi.org/10.1016/j.jtbi.2017.11.014

PERMISSIONS

https://www.elsevier.com/about/our-business/policies/sharing

Accepted Manuscript

Authors can share their accepted manuscript:

[…]

After the embargo period

- via non-commercial hosting platforms such as their institutional repository
- via commercial sites with which Elsevier has an agreement

In all cases accepted manuscripts should:

- link to the formal publication via its DOI
- bear a CC-BY-NC-ND license – this is easy to do, click here to find out how
- if aggregated with other manuscripts, for example in a repository or other site, be shared in alignment with our hosting policy
- not be added to or enhanced in any way to appear more like, or to substitute for, the published journal article

18 June 2019

---

http://hdl.handle.net/2440/111649

Understanding interactions between populations: individual based modelling and quantification using pair correlation functions

S. Dini[1]*, B. J. Binder[1], and J.E.F. Green[1]

[1] School of Mathematical Sciences,
The University of Adelaide,
Adelaide, SA, 5005, Australia

November 1, 2017

Abstract

Understanding the underlying mechanisms that produce the huge variety of swarming and aggregation patterns in animals and cells is fundamental in ecology, developmental biology, and regenerative medicine, to name but a few examples. Depending upon the nature of the interactions between individuals (cells or animals), a variety of different large-scale spatial patterns can be observed in their distribution; examples include cell aggregates, stripes of different coloured skin cells, *etc*. For the case where all individuals are of the same type (*i.e.*, all interactions are alike), a considerable literature already exists on how the collective organisation depends on the inter-individual interactions. Here, we focus on the less studied case where there are two different types of individuals present. Whilst a number of continuum models of this scenario exist, it can be difficult to compare these models to experimental data, since real cells and animals are discrete. In order to overcome this problem, we develop an agent-based model to simulate some archetypal mechanisms involving attraction and repulsion. However, with this approach (as with experiments), each realisation of the model is different, due to stochastic effects. In order to make useful comparisons between simulations and experimental data, we need to identify the robust features of the spatial distributions of the two species which persist over many realisations of the model (for example, the size of aggregates, degree of segregation or intermixing of the two species). In some cases, it is possible to do this by simple visual inspection. In others, the features of the pattern are not so clear to the unaided eye. In this paper, we introduce a pair correlation function (PCF), which allows us to analyse multi-species spatial distributions quantitatively. We show how the differing strengths of inter-individual attraction and repulsion between species give rise to different spatial patterns, and how the PCF can be used to quantify these differences, even when it might be impossible to recognise them visually.

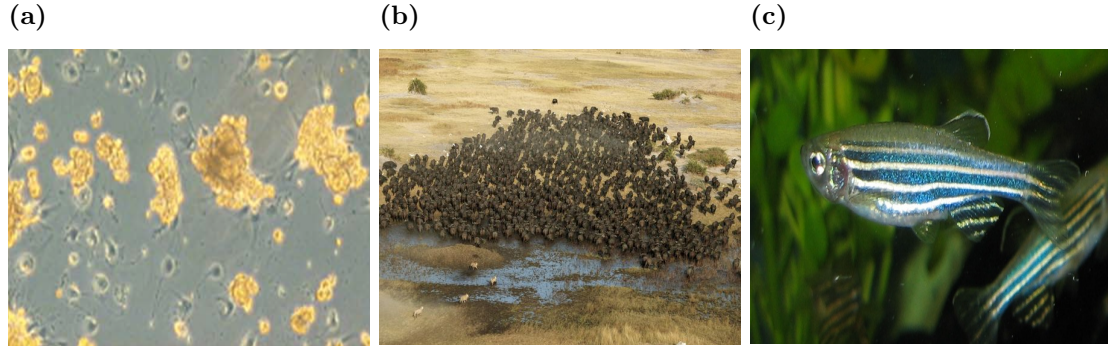
*Email: saber.dini@adelaide.edu.au

Figure 1: Examples of multi-species spatial patterns. (a) Hepatocyte-stellate cells co-cultured to produce spheroids as fundamental part of liver (reprinted from Thomas *et al.* (2006), with permission from Eur. Cells Mater). (b) Lions hunting buffalo on the Duba Plains (image by Beverly Joubert, beverlyjoubert.com). (c) Pattern formation on the skin of a zebrafish (image from Wikipedia).

1   Introduction

There are numerous instances in nature where individuals interact so as to produce a large-scale pattern, such as in the migration of flocks of birds, swarming of bees, foraging in ants, or cells in a developing tissue, *etc.* One longstanding question is to understand how the variety of patterns emerge from relatively simple underlying interactions between the individuals [3]. Commonly, the types of interactions considered are restricted to attraction and repulsion, arising as responses to a range of external stimuli such as those received by the sensory organs of animals (*e.g.* seeing a predator, smelling food resources, *etc.* [49]), or, on the cellular level, resulting from chemical gradients and / or mechanical forces [11, 53]. Patterns such as swarms or cell aggregates may be produced where only a single species is present. However, when individuals of multiple species are present, the potential variety of patterns is greatly increased, as a result of variations in the degree of intermixing or segregation of the species. Three examples, where in each case two different types of individuals are present, are shown in Fig. 1. Fig. 1a shows a co-culture of stellate cells and hepatocytes (two types of liver cell), where stellate cells pull the hepatocytes into aggregated spheroids [53]; Fig. 1b shows three lions chasing a buffalo herd, where the buffalo try to escape and the herd pattern changes accordingly; and Fig. 1c shows an image of a stripe pattern on the skin of a zebrafish formed by two differently-coloured types of cell (xanthophores and melanophores) [23, 24, 50].

Mathematical models have made significant contributions to our understanding of how different types of inter-individual interactions can lead to different large-scale patterns. Well known examples include the reaction-diffusion model of morphogenesis, introduced by Turing (1952) (which was later applied to animal coat patterns by Murray [43, 44, 42]), and the chemotaxis model presented by Keller and Segel (1970) which produced new insights into the mechanisms underpinning the formation of cell aggregates in dictyostelium (and many other cell types). In many mathematical models, the underlying interactions between the individuals are idealised as being combinations of attraction and repulsion [36]. The interplay between these opposing forces influences the pattern. For example, Mogilner *et al.* (2003) shows that short-ranged repulsion combined with long-range attraction is necessary to produce cohesive and well-spaced groups in a population of a single species (similar works can be found in [10, 15, 55]). At the cellular level, a variety of factors which would produce these types of interactions, such as

chemo- attractants / repellents [31], traction forces [19], volume exclusion [4], *etc.*, have been investigated. For predator-prey interactions, a model is proposed by Chen and Kolokolnikov (2014), where different behaviours depending on the strength of attraction between the prey and predator are discussed.

The modelling approaches used to study pattern formation can broadly be divided into continuum and agent-based. Continuum models are formulated in terms of the densities of the species of interest, functions of space and time which obey systems of partial differential equations (PDEs). They have the advantage that analytical techniques, such as linear stability analysis, can be used to understand aspects of their behaviour over the entire parameter space, which can help to give insight into the mechanisms underpinning particular phenomena. Examples would include the non-local (integro-PDE) models introduced by Mogilner and Edelstein-Keshet (1999) for the study of swarms. In this kind of model, movement of an individual is influenced by superposition of the forces exerted by the surrounding individuals. These forces are represented by a convolution integral in this continuum framework [19, 20, 48]. Although the continuum models provide good population-level information on pattern formation, because individuals are discrete, it is difficult to compare their predictions with experiments on anything other than a qualitative level [19].

In contrast to continuum models, agent-based models (ABMs) represent each individual explicitly. ABMs are more realistic in this sense, as they allow us to consider individual level behaviour, which usually includes an element of stochastic behaviour (*e.g.* [12, 35, 37, 46]). However, this comes at higher computational cost. In this work we develop an ABM with two species of agents to study the interactions between the individuals. The model developed here builds upon the earlier work for the one-species case described in [1, 12].

The fact that stochasticity can play a role in the distribution of the individuals presents a challenge. Each realisation of the process (*i.e.* simulation of the model) will be different, owing to differences in the (random) initial conditions, or the randomness inherent in the interactions (even when the interaction rules are fixed). We need to be able to identify which features of the spatial pattern are robust (*i.e.*, recur in many realisations of the process). As a first step, this requires suitable statistical tools to quantify the spatial distributions of individuals so that we can compare the patterns observed in different experimental or simulated datasets. Pair correlation functions (PCFs) are popular candidates for statistical analysis of individuals patterns [13, 22]. PCFs quantify spatial patterns by showing deviations from complete spatial randomness (CSR), where the individuals are distributed uniformly at random. They describe the frequency of pairs of individuals separated by a certain distance, relative to what is expected for CSR [5]. PCFs are increasingly being used to quantify cell distributions [6, 14, 16, 40, 56] and have recently been shown to have advantages over one of the most commonly used computational methods for quantifying spatial distributions that are close to CSR [14]. Agnew *et al.* (2014) suggest that the PCF can be used to distinguish between the spatial patterns that arise from cell aggregate formation due to cell proliferation, and those where the aggregates form as a result of cell-cell attraction (*e.g.*, due to chemotaxis).

Here, we follow the approach presented by [5] for quantifying single-species volume exclusion processes. We extend their method to develop a PCF for multi-species volume exclusion processes on a two-dimensional Cartesian lattice. The method is based on normalising the frequency of pairs by finding their expected values for the uniform distribution [5]. Periodic continuation is applied in order to eliminate boundary effects [22]. We then compute the PCF for realisations of our ABM simulated using different sets of parameter values (strengths and ranges of attraction and repulsion). The PCF allows us to characterise various spatial features

from the patterns, such as intensity of clustering, spacing between the clusters, *etc.* We demonstrate how the parameter values in the model can be related to the PCF calculated from the model output (averaged over a number of realisations). This suggests ways in which the models can be fitted to data [25, 51, 54].

Using the ABM and PCF developed in this work, we analyse two types of inter-species interactions: mutually attractive (or repulsive) and attractive-repulsive. For the case of mutually attractive (or repulsive) systems, we examine the generic behaviour for short length scale interactions, and the results suggest strong heterotypic repulsion is a necessary requirement for the emergence of large length scale patterning in which clusters are not distributed uniformly at random throughout the spatial domain. In the second case of attractive-repulsive systems, we consider both predator-prey systems and stripe formation on the skin of zebrafish. Our analysis of predator-prey systems suggests that strong homotypic attraction between prey, which produces the herd like behaviour commonly observed in predator-prey systems [39, 41], may not be the optimal strategy to minimise predation overall. With regards to stripe formation in zebrafish, we demonstrate that it is possible to produce stripes with no homotypic interactions, and this is in contrast to the existing analysis of Painter *et al.* (2015) and Woolley *et al.* (2014), who both suggest that homotypic interactions are necessary for stripe formation.

2 Model and quantification method

2.1 Multi-species agent-based model

In this paper, we simulate the interactions between individuals (which can be cells, animals, *etc.*) using an ABM. The model used here is an extension of that developed in [1, 12]. Agents move on a discrete two-dimensional lattice (x, y), of dimensions $X \times Y$. Motivated by applications in cell biology, we consider the domain to be periodic, thus, any agent that leave the lattice from one side, re-enters again from the opposite side. We introduce this assumption since in cell biology experiments, only a small 'window' is observed (corresponding to the field of view of the microscope), which generally does not include the edge of the well in which the cells are cultured. We consider that, on average, a cell moving outside the field of view is likely to be replaced by another moving into it, which is approximated by adopting periodic boundary conditions. Such boundary conditions eliminate edge effects, allowing us to focus on the effects of different types of inter-individual interactions. In this work, we restrict our attention to the case where there are only two types of agents.

Agents move on the lattice according to two motion rules: biased motion (with probability P_b) and unbiased random motion (with probability $1 - P_b$). In unbiased random motion, an agent attempts to move to one of its four neighbouring sites with equal probability. In biased motion, the probability of moving to each of the neighbouring sites is affected by the fact that an agent can sense the number of other agents within a certain range. The probabilities are calculated based on the rules of attraction and repulsion which are assumed to operate between agents of the specific types involved. Note that each site can only be occupied by only one agent at a time; if a agent attempts to move into an occupied site, the move is aborted. The model thus takes account of volume exclusion ([4, 52]).

In the case of biased motion, we need to define and calculate the probability of movement to each of the four neighbouring lattice sites. We denote this probability by P_k, where k indicates the direction of attempted movement: $k = 1$ - right, $k = 2$ - left, $k = 3$ - up, and $k = 4$ - down, where $\sum P_k = 1$. We assume that agents of type m are attracted (repelled) by agents of

type p within a range α_{mp} (γ_{mp}), where $m, p \in \{1, 2\}$. Fig. 2 shows how the agents sense their neighbours within a certain range and in a specific direction. We take the bias probability to depend only upon the number of agents of each type within the relevant attraction / repulsion ranges in each of the four directions.
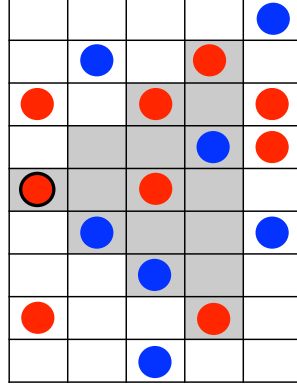

Figure 2: Directional neighbourhood of an agent. A sample two-species pattern is depicted with the red ('1') and blue ('2') colours. For example, for the red agent marked out with the black border $E_{11}(\alpha_{11}) = 4, E_{12}(\alpha_{12}) = 3$, where $\alpha_{11} = \alpha_{12} = 3$ is the range of attraction shown by the shaded sites.

The probability of moving in each of the four directions, P_k, is calculated from a four-dimensional directional bias vector, $\boldsymbol{v}$. We define this for each agent at each timestep as

$$\boldsymbol{v} = \boldsymbol{A}\boldsymbol{a} + \boldsymbol{R}\boldsymbol{r},$$

where $\boldsymbol{A}$ ($\boldsymbol{R}$) is a matrix whose entries are the number of neighbouring agents within the attraction (repulsion) range and $\boldsymbol{a}$ ($\boldsymbol{r}$) is a two-dimensional weight of attraction (repulsion) vector. These, in turn, are defined as follows. For an agent of type m (where $m = 1$ or 2), $\boldsymbol{A}$ is given by

$$\boldsymbol{A} = \begin{bmatrix} E_{mm}(\alpha_{mm}) & E_{mp}(\alpha_{mp}) \\ W_{mm}(\alpha_{mm}) & W_{mp}(\alpha_{mp}) \\ N_{mm}(\alpha_{mm}) & N_{mp}(\alpha_{mp}) \\ S_{mm}(\alpha_{mm}) & S_{mp}(\alpha_{mp}) \end{bmatrix}, \qquad \text{for} \quad m, p \in \{1, 2\},\ m \neq p,$$

where $E_{mm}(\alpha_{mm})$ is the number of agents of type m to the right of the agent, within the range determined by α_{mm} (see Fig. 2). Similarly, $W_{mm}(\alpha_{mm})$ is the number of agents to the left, $N_{mm}(\alpha_{mm})$ is the number of agents above and S_{mm} is the number of agents below. Likewise, $E_{mp}(\alpha_{mp}), W_{mp}(\alpha_{mp}), N_{mp}(\alpha_{mp})$ and $S_{mp}(\alpha_{mp})$ account for the heterotypic neighbouring agents. The weight of attraction vector is defined by

$$\boldsymbol{a} = \begin{bmatrix} a_{mm} \\ a_{mp} \end{bmatrix},$$

where a_{mm} and a_{mp} are the weights of attraction of agents of type m to agents of the same type and of different type, respectively. Noting that repulsion will produce biases is the opposite direction compared to attraction, for an agent of type m, $\boldsymbol{R}$ and $\boldsymbol{r}$ are similarly defined to be:

$$\boldsymbol{R} = \begin{bmatrix} W_{mm}(\gamma_{mm}) & W_{mp}(\gamma_{mp}) \\ E_{mm}(\gamma_{mm}) & E_{mp}(\gamma_{mp}) \\ S_{mm}(\gamma_{mm}) & S_{mp}(\gamma_{mp}) \\ N_{mm}(\gamma_{mm}) & N_{mp}(\gamma_{mp}) \end{bmatrix}, \qquad \text{for} \quad m, p \in \{1, 2\},\ m \neq p,$$

and

$$\boldsymbol{r} = \begin{bmatrix} r_{mm} \\ r_{mp} \end{bmatrix},$$

where r_{mm} is the weight of homotypic (same type) repulsion for agents of type m and r_{mp} is the weight of heterotypic (different type) repulsion between agents of type m and p.

Finally, we calculate the probability of moving in each of the four directions, P_k, by normalising $\boldsymbol{v}$:

$$P_k = \frac{v_k}{\sum\limits_{q=1}^{4} v_q}, \quad \text{for} \quad k = 1, 2, 3, 4. \tag{2.1}$$

Thus, the direction in which the agent will tend to move (reflected by P_k) is determined by the interplay of homotypic and heterotypic attraction and repulsion influences.

We simulate the model as follows. During a discrete time-step, each agent is selected in random sequential order and is given the opportunity to move either according to the unbiased or biased motion rule. For an agent located at (x, y), the nature of the motion is determined by generating a random number r_1 from a uniform distribution with support $[0, 1]$. If $r_1 \in [0, P_b)$ the agent attempts to move according to the biased motion rule; otherwise, the motion is unbiased and it attempts to move with equal probability to one of its four neighbouring sites $(x \pm 1, y \pm 1)$. In the case of biased motion, we generate a second random number r_2 from a uniform distribution with support $[0, 1]$, and calculate the values of P_k using Eqn. (2.1). The agent moves to $(x + 1, y)$ if $r_2 \in [0, P_1)$, $(x - 1, y)$ if $r_2 \in (P_1, P_1 + P_2]$, $(x, y + 1)$ if $r_2 \in (P_1 + P_2, 1 - P_4)$ and $(x, y - 1)$ if $r_2 \in (1 - P_4, 1]$. Note that if the agent attempts to move to a site that is occupied by another agent, then that move is aborted, and one aborted movement is counted. These processes are repeated until the spatial distribution of agents evolves to a quasi-steady state, which is determined by examining the evolution of the number of aborted moves in the simulation [1].

2.2 Pair correlation function

We use PCFs as a means to characterise the spatial patterns generated by the ABM simulations. PCFs characterise spatial patterns by showing deviations from CSR (where agents are distributed uniformly at random) [22]. The deviations characterise different spatial features such as the lengthscales of aggregation (or segregation) which are affected by the mechanisms underlying the interactions between individuals. Computing the PCF for a sufficiently large number of realisations of the same experiment can thus potentially provide us with information about these mechanisms.

Binder and Simpson (2013) presented a method to compute the PCF for single-species distributions on lattice. In their method, the normalisation factor, which is the expected value of the number of pairs separated by a certain distance in CSR, is computed for distances in the x and y direction (not the Euclidean distance). Then, the number of pairs occurring in the pattern of interest is divided by the corresponding normalisation factor to give the PCF. Here, we use the same approach and derive the relevant formulae for computing the PCF on periodic domains populated with two (or potentially more) species of agents. Note that the restriction to periodic domains is motivated by the application to cells biology experiments, as explained in §2.1 (we assume our domain represents a 'window' onto a larger domain in which the interactions occur). A further advantage of making this assumption is that PCFs estimated for patterns on finite

domains have significant errors for large distances, whereas periodic continuation helps to mitigate this problem [22]. (Henceforth a reference to a PCF in this paper should be taken to imply one derived assuming periodic boundary conditions.) Our PCFs are defined for homotypic and heterotypic pairs. Indicating the two types of agent by '1' and '2', we denote the PCFs for the 1-1, 2-2 and 1-2 pairs g_{11}, g_{22} and g_{12} respectively. In addition, since the methods for x and y distances are identical, for brevity we present only the formulae for the x direction.

The PCF in the x direction can be defined as

$$g_{mp}(i) = \frac{c_{mp}(i)}{\hat{c}_{mp}(i)}, \quad \text{for} \quad m, p \in \{1, 2\}, \tag{2.2}$$

where $c_{mp}(i)$ is the number of pairs a distance i apart and $\hat{c}_{mp}(i)$ is the normalization factor. $c_{mp}(i)$ for any pattern is obtained by counting the number of pairs with distance i in the x direction and it can be mathematically formulated as

$$c_{mp}(i) = \sum_{l=1}^{N_m} \sum_{j=J}^{N_p} \mathbf{1}_i(|x_l^{(m)} - x_j^{(p)}|), \quad J = \begin{cases} l+1, & m = p, \\ \\ 1, & m \neq p, \end{cases} \tag{2.3}$$

where $x_l^{(m)}$ is the x-coordinate of the lth cell of type m. N_m and N_p are the populations of the species m and p respectively and $\mathbf{1}_i(x)$ is the indicator function defined as

$$\mathbf{1}_i(x) = \begin{cases} 1, & x = i, \\ \\ 0, & \text{otherwise.} \end{cases}$$

The expected number of pairs a distance i apart for CSR can be written in terms of the probability of observing the pairs, given by

$$\hat{c}_{mp}(i) = M_{mp} \, P_{mp}(i),$$

where M_{mp} is the total number of m-p pairs and $P_{mp}(i)$ is the probability that an m-p pair occurs in the lattice. M_{mp} is given by

$$M_{mp} = \begin{cases} \dfrac{N_m(N_m - 1)}{2}, & \text{if} \quad m = p, \\ \\ N_m N_p, & \text{if} \quad m \neq p. \end{cases}$$

The difference in M_{mp} for m-m and m-p is due to the permutation of heterotypic pairs.

In a lattice of width X and height Y, $P_{mp}(i)$ can be found by the ratio of the number of pairs of lattice sites distance i apart, $\hat{d}_{mp}(i)$, to the total possible pairs, given by

$$P_{mp}(i) = \begin{cases} \dfrac{\hat{d}_{mp}(i)}{\frac{1}{2}XY(XY - 1)}, & \text{if} \quad m = p, \\ \\ \dfrac{\hat{d}_{mp}(i)}{XY(XY - 1)}, & \text{if} \quad m \neq p. \end{cases} \tag{2.4}$$

All of the possible pairs that may be observed in a lattice of size $X = 6$ and $Y = 2$ are shown in Fig. 3, for the sake of illustration. As this figure shows, the number of possible pairs of lattice sites distance i apart in one row is

$$\hat{r}_{mm}(i) = X, \quad \text{for} \quad i = 1, ..., \frac{X}{2} - 1.$$

Here, we assumed X and Y are even, however, the method is the same for odd X and Y for distances $i = 1, ..., (X-1)/2$.

Note that if the two agents were of different types, each possible pair shown in Fig. 3 should be counted twice due to the possible permutation between them. Thus, for m-p pairs the counts should be multiplied by two, i.e. $\hat{d}_{mp} = 2\hat{d}_{mm}$, $m \neq p$.

Then, the possible number of pairs that can occur when there are multiple rows is given by

$$\hat{d}_{mm}(i) = \hat{r}_{mm}(i)Y + 2\hat{r}_{mm}(i)\binom{Y}{2} = Y^2 X, \quad \text{for} \quad i = 1, ..., \frac{X}{2} - 1,$$

where the first term at the RHS of the above equation accounts for the Y cases where the paired points are in one row (Figs. 3a and 3b), and the second term accounts for the paired points in different rows (Figs. 3c and 3d).
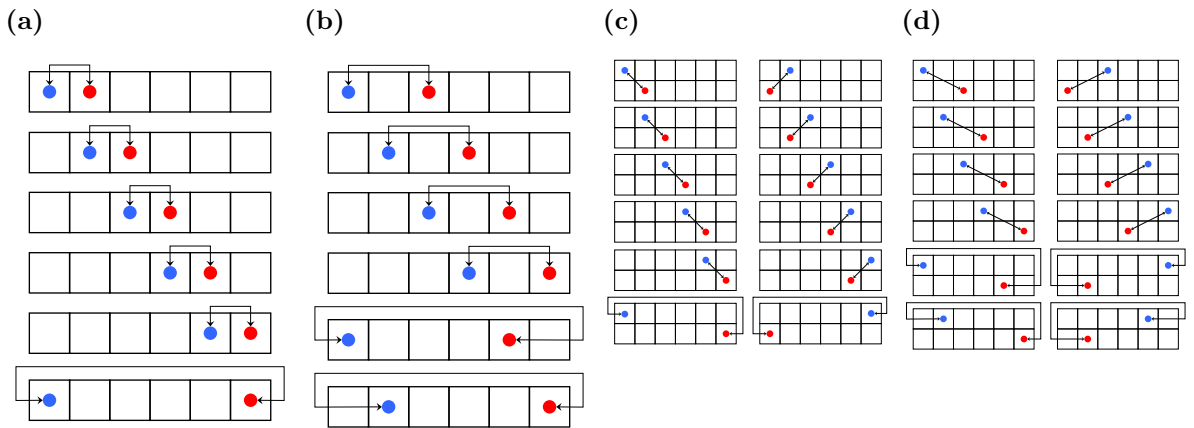

(a) **(b)** **(c)** **(d)**

Figure 3: All possible combinations of pairs of sites in a lattice with $X = 6$ and $Y = 2$. The arrows depict the distances which can be direct or periodic. The pairs of unit distance apart in (a) one row and (c) two rows. The pairs of distance two apart in (b) one row and (d) two rows.

Finally, substituting $\hat{d}_{mm}(i)$ into Eqn. (2.4), yields the normalisation factor:

$$\hat{c}_{mp}(i) = \begin{cases} \dfrac{N_m(N_m - 1)Y}{XY - 1}, & \text{if} \quad m = p, \\ \dfrac{2N_m N_p Y}{XY - 1}, & \text{if} \quad m \neq p. \end{cases} \quad (2.5)$$

Thus, by computing $c_{mp}(i)$ defined in Eqn. (2.3), the normalising factor $\hat{c}_{mp}(i)$ in Eqn. (2.5) and plugging them into Eqn. (2.2), we are able to evaluate the PCF for a given pattern.

For a spatial domain that is populated uniformly at random the expected value of the PCF is unity at all distances. When the PCF is greater than unity at some distance we have aggregation, and when the PCF is less than unity at some distance we have segregation. In the following section, we use the PCF to identify homotypic and heterotypic aggregation / segregation length-scales in three examples of two-species spatial patterns.
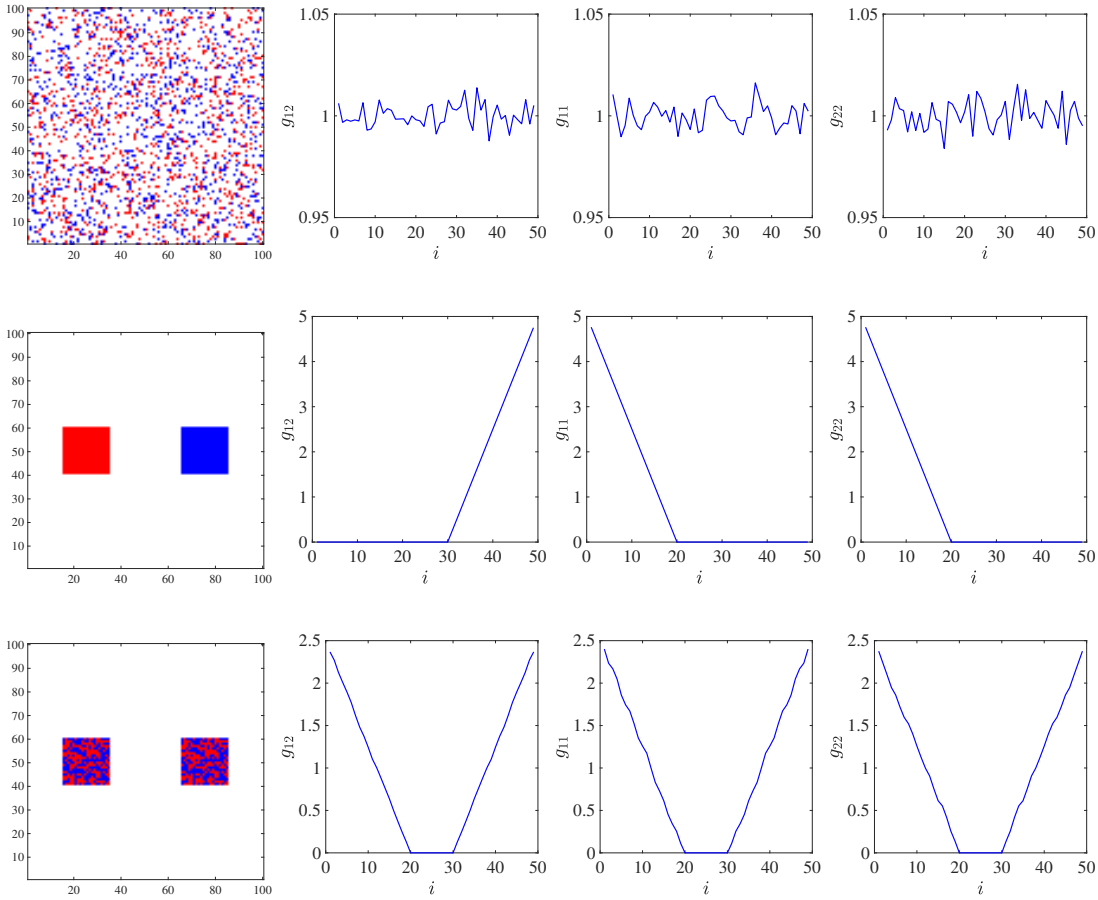
Figure 4: Three two-species patterns and their PCFs in the x direction, $N_1 = N_2 = 400$. First column of panels: From top to bottom, the agents are distributed uniformly at random, in two segregated clusters and in two intermixed clusters. Second column of panels: Heterotypic PCFs. Third column of panels: Homotypic PCFs for the red species. Fourth column of panels: Homotypic PCFs for the blue species.

2.3 Illustrative two-species spatial patterns

We begin by evaluating the PCFs in the x direction for the patterns shown in the first column of Fig. 4 (illustrations of the PCF for a variety of one-species patterns can be found in [5] for comparison). Understanding how information about the pattern is encoded in the PCF for these examples will help to guide our interpretation of the PCF in the more complex situations which are presented in §3. We follow the practice found in earlier papers [1, 5] and use linear interpolation to represent the discrete PCFs as continuous curves (columns 2-4 in Fig. 4).

The first example we consider is where the two species are distributed uniformly at random, as is illustrated in the first row of Fig. 4. As expected, we observe that the heterotypic and homotypic PCFs have a small-amplitude oscillation around unity, indicating that there is no heterotypic or homotypic spatial structure in the pattern. This provides a check on the derivation of the PCFs, which were normalised with respect to CSR.

In the second example, individuals of the same type are distributed in two single-species clusters (red and blue squares in second row Fig. 4). The heterotypic PCF is equal to zero for

9

$0 < i \leq 30$ (as the two clusters are 30 units apart), and then increases linearly for $30 < i \leq 50$ (as each cluster is 20 units in length) to a maximum value at $i = 50$ (the distance between the two centres of the clusters). Therefore, there is heterotypic segregation at short to intermediate distances and heterotypic aggregation at large distances. In contrast, both homotypic PCFs indicate short to intermediate scale aggregation only, for $0 < i \leq 20$.

For the third and final example, the two-species are distributed uniformly at random within two clusters and the heterotypic and homotypic PCFs are all the same (third row of Fig. 4). Additionally, the interpretation of the PCFs is similar to that of the PCF for the single-species clustering pattern in Figure 4 of [5]. Subsequently, the heterotypic, homotypic and overall population aggregation / segregation length-scales are also all the same. We observe short scale aggregation ($0 < i \leq 20$), intermediate scale segregation ($20 < i \leq 30$), and long scale aggregation ($30 < i \leq 50$).

3   Results

Having described our modelling approach and quantification method, we are now in a position to investigate the types of patterns produced by different combinations of inter-individual interactions, and the extent to which different pattern-forming mechanisms can be distinguished by analysis of the resulting pattern using the PCF. For each set of results in Figs. 5–8, we evaluate the average PCFs in the x direction for $N = 60$ simulations that have evolved to a quasi-steady state from initial conditions where both species were distributed uniformly at random throughout the domain. As in Agnew *et al.* (2014), we use the number of aborted movements as the measure of reaching the quasi-steady state. The layout of Figs. 5–8 is similar to that of Fig. 4, with the additional broken curves representing the 95% confidence intervals of the t-distribution for the average PCFs (solid curves). In all the simulations, we choose a high value of the probability of biased motion, $P_b = 0.8$, which allows us to focus our study on cell interactions effects, rather than the effect of unbiased motion. Also, the ranges of attraction and repulsion are set to $\alpha_{mp} = \gamma_{mp} = 5$, further concentrating the majority of our investigation on the effect of varying the strengths of attraction and repulsion, a_{mp} and r_{mp}. This restriction is relaxed in the last set of results (Fig. 9), where we study the effect of varying the ranges of attraction / repulsion in the system. Similar sets of results are found for the average PCFs in the y direction, as the interactions and initial conditions make no difference between the x and y directions. We consider two generic types of inter-species interactions: mutually attractive (or repulsive) and attractive-repulsive.

3.1   Mutually attractive or repulsive inter-species interactions

The first case we consider is where the inter-species interactions are either mutually attractive or repulsive (*i.e.*, type 1 agents are attracted to (repelled by) type 2 agents, and type 2 agents are attracted to (repelled by) type 1 agents). This is motivated by observations of co-cultured hepatocytes and stellate cells *in vitro*, which produce cell aggregates (see Fig.1a). The experiments undertaken by Thomas *et al.* (2006) indicate that in co-culture, cluster formation is enhanced compared to hepatocyte only culture (see the images and videos in [53]). A continuum model of this process was developed by Green *et al.* (2010). They assumed attractive interactions between hepatocytes, and mutually attraction between hepatocytes and stellates. (Short range repulsion between cells of all types was also included in the model, to represent the effect of overcrowding at high cell densities.) Depending upon the relative strength of hepatocyte-hepatocyte

and hepatocyte-stellate interaction, the model found that cells formed clusters within which the two types were either segregated, partially-segregated, or intermixed. We will consider similar scenarios here using our model, which has the advantage over continuum models of representing the cells as discrete entities, and including the effects of crowding more naturally (since only once agent can occupy each lattice site).

3.1.1 Heterotypic interactions only

We begin by analysing a system governed by heterotypic interactions only (so $a_{11} = a_{22} = r_{11} = r_{11} = 0$) and where the strengths of attraction and repulsion are the same for both species $a_{12} = a_{21}$, $r_{12} = r_{21}$. Thus, interactions between agents of the same type are governed simply by volume exclusion (as only one agent can occupy a lattice site). The strengths of heterotypic attraction and repulsion are then varied, and the results are presented in Fig. 5.

When attraction is much stronger than repulsion clusters are formed in which the two species intermix, as shown in the first row of Fig. 5. The PCF for this type of pattern can be interpreted by considering the illustrative example in the last row of Fig. 4 and the one-species patterns found in [1, 5]. Similar to the results in the last row of Fig. 4, the heterotypic and homotypic PCFs are almost identical and therefore the heterotypic, homotypic and overall population (*i.e.* ignoring agents types) aggregation / segregation length-scales are also all the same. The values of the PCFs above unity at short distances indicate short scale aggregation (*i.e.* the clusters in the first row of Fig. 5), with the minimum in the PCFs at $i \approx 10$ providing a quantitative measure of the average spacing between the clusters, or the scale of segregation. The fact that the three PCFs are the same shows that there are no significant differences in the distributions of the two species, indicating they are intermixed uniformly at random within each cluster. At intermediate and large distances, for $i > 20$, the PCFs are close to unity, implying that the centres of the clusters are distributed uniformly at random, as observed for the one-species patterns in [1, 5].

When repulsion is much stronger than attraction clusters are again produced, but in this case the species are now segregated, so that the red and blue agents are no longer intermixed (see fourth row of Fig. 5). The clusters are also no longer compact and roughly circular, but elongated, eccentric shapes. However, the fundamental characteristics of the PCFs are similar to those for the illustrative example in the second row of Fig. 4. Where heterotypic aggregation / segregation occurs, we observe homotypic segregation / aggregation. In other words, the heterotypic and homotypic PCFs are in anti-phase. For example, at the distance $i \approx 10$ there is maxima in the heterotypic PCF and a minima in both the homotypic PCFs (fourth row of Fig. 5).

Unlike the case of strong attraction where there is heterotypic aggregation at short-distances (first row of Fig. 5), in the case of strong repulsion we observe short-scale heterotypic segregation (fourth row of Fig. 5). Furthermore, for strong repulsion we observe heterotypic and homotypic aggregation / segregation at large distances, which is in contrast to the lack of spatial structure at large distances when compared to that of strong attraction.

The above discussion shows that the PCFs can distinguish and characterise either strong attraction or strong repulsion heterotypic interactions that produce visible spatial clustering. We now consider the case of weak attraction and weak repulsion that generate patterns with no visible spatial structure (see second and third row of Fig. 5). In the case of weak heterotypic interactions, the deviations of the maximum and minimum values of the PCFs from unity are at least an order of magnitude smaller than those for the case of strong heterotypic interactions,
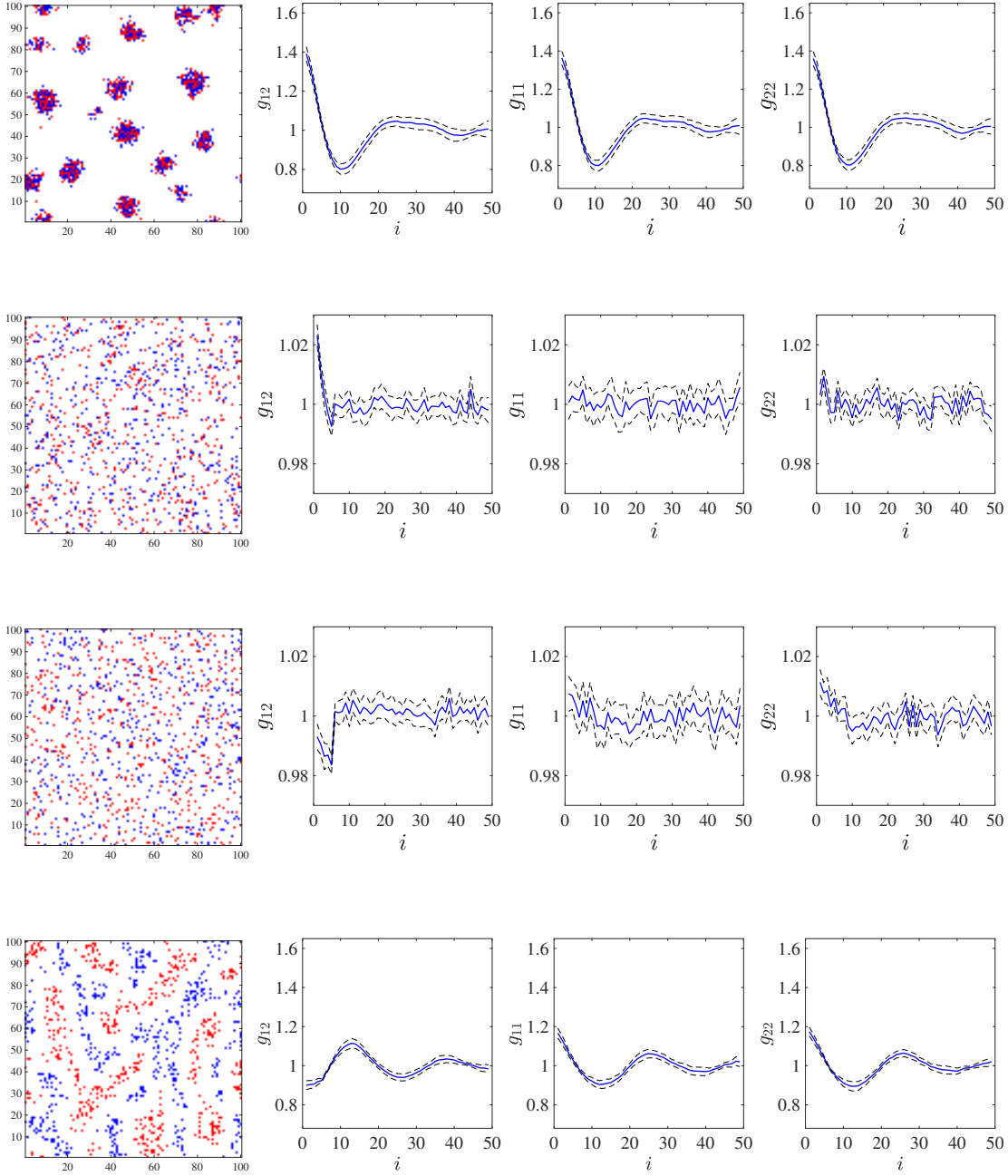
Figure 5: Mutually attractive or repulsive species with heterotypic interactions only, $a_{11} = a_{22} = r_{11} = r_{11} = 0$ and $N_1 = N_2 = 500$. First row: Strong heterotypic attraction, $a_{12} = a_{21} = 5$ and $r_{12} = r_{21} = 1$. Second and third row: Weak heterotypic attraction and repulsion. Second row: $a_{12} = a_{21} = 1.2$ and $r_{12} = r_{21} = 1$. Third row: $a_{12} = a_{21} = 1$ and $r_{12} = r_{21} = 1.2$. Fourth row: Strong heterotypic repulsion, $a_{12} = a_{21} = 1$ and $r_{12} = r_{21} = 5$.

12

indicting that the patterns are close to CSR. However, even with a relatively small number of simulations ($N = 60$), the heterotypic PCFs correctly identify the weak, short scale behaviour. For example, in the second row of Fig. 5 the heterotypic attraction ($a_{12} = a_{21} = 1.2$) is slightly stronger than the heterotypic repulsion ($r_{12} = r_{21} = 1$) and we observe weak short scale heterotypic aggregation, similar to that found for strong attraction in the first row of Fig. 5.

These few examples clearly illustrate the potential usefulness of the PCF for identifying the presence of attractive (or repulsive) heterotypic interactions, even when no pattern is distinguishable by eye. However, they also sound a note of caution in using the PCF to infer the mechanism of pattern formation. The fact that the homotypic PCFs are above unity at short distances in the first and fourth rows of Fig. 5 is not indicative of homotypic attraction; it occurs because agents of the same type are forced together by strong attractive, or repulsive heterotypic interactions. Thus, if we wish to try to make inferences about the mechanism of pattern formation from the PCFs, we need to consider the heterotypic and homotypic PCFs simultaneously, and may require information about the homotypic interactions (*e.g.* from an experiment where only one species is present).

3.1.2 Homotypic interactions only

We now investigate the patterns which can occur with only homotypic interactions between the two species (so $a_{12} = a_{21} = r_{12} = r_{21} = 0$), with the same strengths of attraction and repulsion for each species $a_{11} = a_{22}$ and $r_{11} = r_{22}$. The results for strong homotypic attraction and strong homotypic repulsion are presented in the first and second row of Fig. 6.

For strong attraction, we observe short scale heterotypic segregation, short scale homotypic aggregation, intermediate scale heterotypic aggregation and intermediate scale homotypic segregation (first row of Fig. 6). We remark that the short scale heterotypic segregation is not indicative of heterotypic repulsion (as $r_{12} = r_{21} = 0$), and is instead the result of the strong homotypic attraction which pulls species of the same type together. We also see that the heterotypic PCF is quite similar to that of the system with only heterotypic repulsion (see fourth row of Fig. 5). However, at intermediate and large distances, the homotypic PCFs in the system with only homotypic interactions are quite different from those of the system with only heterotypic interactions. This is because the compact clusters are distributed uniformly at random in the first row of Fig. 6 (as shown by the fact that the PCFs are close to unity at large distances), whereas the elongated clusters are distributed in a segregated pattern in the fourth row of Fig. 5 (as the PCFs show noticeable fluctuations about unity at large distances). Hence, as mentioned earlier, this warrants the use of the homotypic PCFs in identifying the dominant underlying interactions along with the heterotypic PCF.

Strong repulsion produces patterns with almost no visible spatial structure (second row of Fig. 6). The heterotypic PCF shows that the inter-species distribution is close to CSR, whilst the homotypic PCFs reveal weak short scale homotypic segregation, due to the dominance of homotypic repulsion.

3.1.3 Heterotypic and homotypic interactions

We now consider an example of when both homotypic and heterotypic interactions are present in the system, and focus our attention on weak homotypic attraction and strong heterotypic repulsion (Fig. 7). When compared to the elongated and segregated clusters in the fourth row of Fig. 5 (*i.e.* , strong heterotypic repulsion only), we see that the effect of weak homotypic
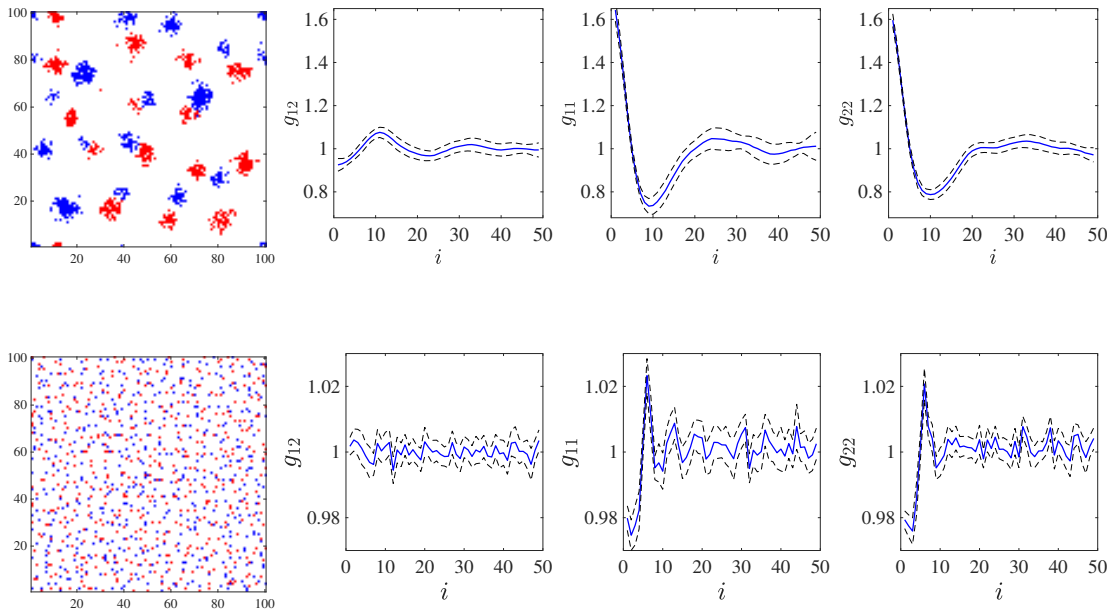
Figure 6: Mutually attractive or repulsive species with homotypic interactions only, $a_{12} = a_{21} = r_{21} = r_{12} = 0$ and $N_1 = N_2 = 500$. First row: Strong homotypic attraction, $a_{11} = a_{22} = 5$ and $r_{11} = r_{22} = 1$. Second row: Strong homotypic repulsion, $a_{11} = a_{22} = 1$ and $r_{11} = r_{22} = 5$.

attraction forms more compact clusters in Fig. 7. At a glance, these compact clusters appear similar to those in the first row of Fig. 6 (*i.e.* strong homotypic attraction only). However, upon closer inspection, the compact clusters in Fig. 7 are not distributed uniformly at random throughout the domain, as is the case for those in the first row of Fig. 6.

To summarise the clustering observed in Figs. 5, 6 and 7, we find that systems with either strong heterotypic or homotypic attraction produce clusters that are distributed uniformly at random, whereas systems with strong heterotypic repulsion produce clusters that are not distributed uniformly random. Therefore, the results suggest strong heterotypic repulsion is a necessary requirement for large length scale patterning in mutually attractive (or repulsive) systems with short length scale interactions. The PCF analysis is consistent with these observations, and further demonstrates the usefulness of the PCFs to quantify multi-species spatial patterns.

3.2 Attractive-repulsive inter-species interactions

We now turn to the case where the heterotypic interactions produce opposite effects on the two species - *e.g.*, species 1 is attracted to species 2, whilst species 2 is repelled by species 1. This type of interaction is termed *run-and-chase*. We consider two examples of run-and-chase interactions that can produce visible clusters of one of the species (*e.g.* prey) and two-species striped patterns (*e.g.* zebrafish skin).
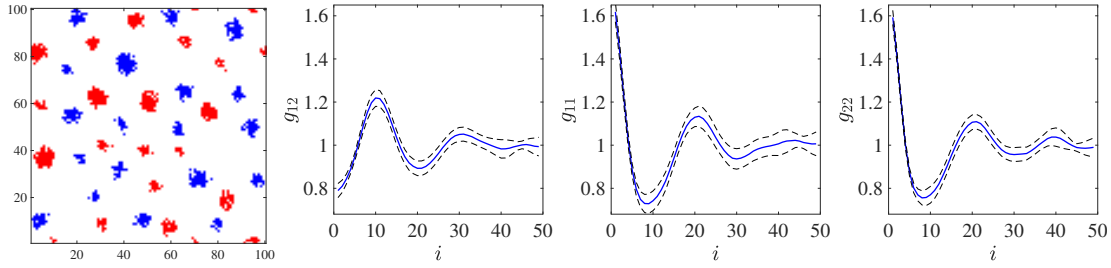
14

Figure 7: Mutually attractive or repulsive species with weak homotypic attraction and strong heterotypic repulsion, $a_{11} = a_{22} = 1$, $r_{12} = r_{21} = 5$, $a_{12} = a_{21} = r_{11} = r_{22} = 0$ and $N_1 = N_2 = 500$.
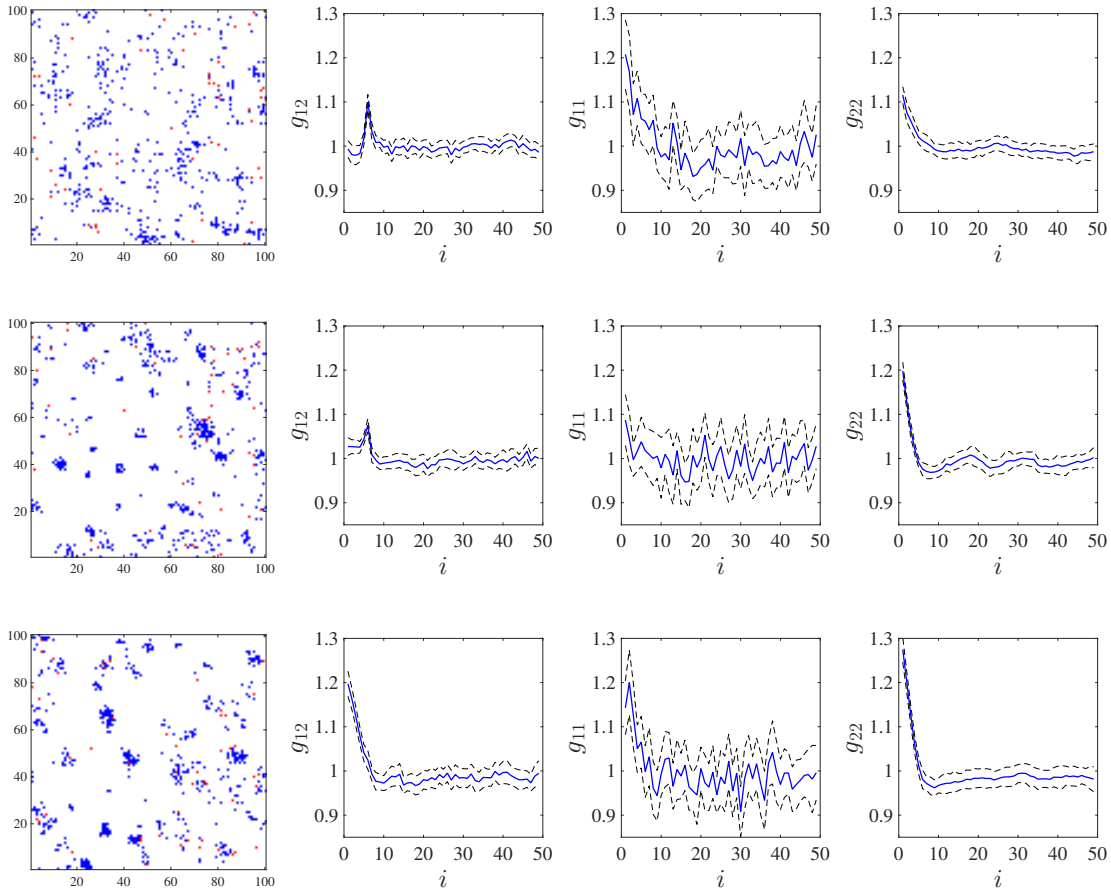

Figure 8: Strong attractive-repulsive interactions with no homotypic repulsion and no predator homotypic attraction, $a_{12} = r_{21} = 50$, $r_{11} = r_{22} = r_{12} = a_{21} = a_{11} = 0$, $N_1 = 50$ and $N_2 = 500$. Predators (red) are attracted to preys (blue). The effect of varying the prey homotypic attraction is shown. First row, $a_{22} = 0$ Second row, $a_{22} = 5$. Third row, $a_{22} = 10$.

3.2.1 Predator-prey system

A common situation where the run-and-chase mechanism pertains is a predator-prey system where predators (species 1) are attracted to prey (species 2), which try to flee from them (Fig. 1b). Various swarming patterns may emerge [9]. Living in a swarm provides a variety of advantages for animals, such as enhanced defensive capabilities, vigilance, foraging, mating success, *etc.* [28, 49], but it can as well have detrimental effects, which are discussed in the following.

The dynamical behaviour of predator-prey systems have been extensively studied [2, 9, 62]. However, the analysis of spatial patterns generated with discrete models of this system has received much less attention. Therefore, we set the parameters of our ABM to mimic a predator-prey system and apply our PCF to the resulting patterns. Obviously, our model does not incorporate all of the underlying mechanisms found in specific predator-prey systems. For example, game theoretical models have been used to examine collective strategies (both prey and predator) found in specific predator-prey systems [8, 29, 32]. Nevertheless, the aim here then is to investigate the behaviour of attractive / repulsive interactions commonly found in most predator-prey systems, and focus on the spatial patterns produced by these systems.

We assume that a smaller group of predators chase a larger group of prey, with strong attractive (predator)-repulsive (prey) heterotypic interactions. We also assume homotypic attraction between prey, to provide group cohesion. All other potential interactions are neglected. We choose much higher heterotypic strengths compared to homotypic ones, based on the idea that for the prey avoiding the predators is of greater importance than staying near to other members of the same species.

The assumption of homotypic attraction between the fleeing prey when attacked by predators is often justified by the 'selfish herd' hypothesis [39, 41]. The hypothesis states that each prey tries to distance itself from the predators by attempting to remain close to the centre of the herd, which would make other individuals more exposed. We use our PCF to investigate the influence of the prey's homotypic attraction on the patterns produced. The results can then be used to discuss the extent to which different behaviours contribute to the success / failure of the prey / predators [47].

The effect of increasing the prey homotypic attraction is shown in Fig. 8 (top-bottom rows). Although the homotypic PCFs are not remarkably different in different experiments, the effect of increasing the prey's homotypic attraction produces a qualitative and quantitative change in the heterotypic PCFs. As shown in the first row of Fig. 8, for $a_{22} = 0$, the maxima of the heterotypic PCF at $i \approx 5$ indicates that large number of prey and predators are 5 sites apart, which can be interpreted as the prey successfully keeping their distance from the predators. But as the homotypic attraction of the prey increases, this maximum at $g_{12}(5)$ decays, while $g_{12}(1)$ becomes dominant (see second row of Fig. 8). Fig. 8 illustrates the dominance of $g_{12}(1)$ for $a_{22} = 10$. This indicates proximity of predators and prey, which is likely to be associated with success for the predators.

These results support the notion that living in a swarm can increase the risk of predation for the prey, by providing a more easily-recognisable target for predators [49]. Importantly, the detrimental effect of homotypic attraction in prey is quantified by the computed PCFs. Our results suggest that homotypic attraction may save individuals by placing others closer to predators, but it works at the expense of increased overall predation. This is shown by the increase in $g_{12}(1)$ with increasing the strength of homotypic attraction, which indicates the increased averaged proximity of predators to the preys.

The quantification approach taken here can be readily applied to more sophisticated predator-prey models that incorporate greater levels of biological detail. We believe this may help to produce insights into the optimum strategies for prey, which minimise the risk of predation.

3.2.2 Zebrafish stripes

The zebrafish is a popular model organism for the study of pattern formation in animals [21, 23, 24, 34, 50]. In particular, we consider the development of the striped pattern on its skin, as is illustrated in Fig. 1c. The two species of interest here are melanophores and xanthophores, two types of pigment cell (dark and light coloured, respectively) which are involved in creating the skin patterns (for simplicity, other cell types such as iridophores [17] are neglected here).

Pattern formation in zebrafish has been analysed using various mathematical models, both continuum [18, 45, 60] and discrete [7, 38, 58]. Recent studies suggest that *run-and-chase* is the major underlying mechanism for stripe formation [23, 61]. It has been observed that melanophores migrate away from the chasing xanthophores when the melanophores contact the dendrites of the xanthophores [23]. We implement a generic run-and-chase scenario in our ABM, and investigate possible patterns and their spatial characteristics. In this work, we concentrate on the effect of cells interactions on stripe formation. Thus, other factors that may impact on this process, such as domain growth, are not considered here (see *e.g.* [58] for a more complex model of stripe formation in zebrafish).

The different patterns generated by varying the heterotypic ranges of attraction and repulsion are illustrated by Fig. 9a where the homotypic interactions are deactivated ($a_{11} = a_{22} = r_{11} = r_{22} = 0$). In these simulations, the escaping agents of type 2 (blue) are being chased by agents of type 1 (red). We vary the range that chasers are attracted to runners, α_{12}, and the range that runners are repulsed by chasers, γ_{21}. Fig. 9b shows the associated heterotypic PCFs, g_{12}. As Fig. 9a indicates, stripes (which can randomly be horizontal or vertical) are formed when $\alpha_{12} = \{10, 15\}$ and $\gamma_{21} = \{1, 5\}$, without any homotypic interactions. This implies that a simple run-and-chase system (without homotypic interactions) is able to produce a striped pattern. The highly deviated g_{12} for $\alpha_{12} = \{10, 15\}$ and $\gamma_{21} = \{1, 5\}$ confirms that these generated patterns are quite distinct from CSR. In addition, the values of g_{12} below unity at short distances demonstrate the segregation of the two types.

The PCFs for $\alpha_{12} = \{10, 15\}$ and $\gamma_{21} = \{1, 5\}$ show that g_{12} magnitude is higher in $\gamma_{21} = 5$ than that in $\gamma_{21} = 1$. This means that increasing γ_{21} can give more pronounced stripes. However, g_{12} for $\alpha_{12} = \{10, 15\}$ and $\gamma_{21} = \{10, 15\}$ lie very close to unity, implying that the stripes are significantly distorted. To sum up, we deduce that increasing γ_{21} can help to form more distinct stripes, provided it is kept significantly lower than α_{12}. Generally, this is equivalent to short range of heterotypic repulsion and long range of heterotypic attraction, which is consistent with what is observed in *in vitro* experiments [23]. Moreover, the results indicate that the number of stripes, which is related to the number of maxima / minima of g_{12}, depends only on α_{12} in the studied cases here. Hence, it appears that repulsion can disrupt stripe formation, but it does not affect the number of stripes.

The patterns and PCFs in Figs. 9a and 9b show that stripes are not formed when $\alpha_{12} \leq \gamma_{12}$. However, as noted earlier, when the range of attraction is larger than the range of repulsion the model is capable of producing the stripes without the need to include homotypic interactions. Painter *et al.* (2015) studied the run-and-chase mechanism by means of a one-dimensional continuous model, assuming equal cell-scale ranges of heterotypic interactions between the cells. Based on their results, they suggest that homotypic attraction is necessary for the production
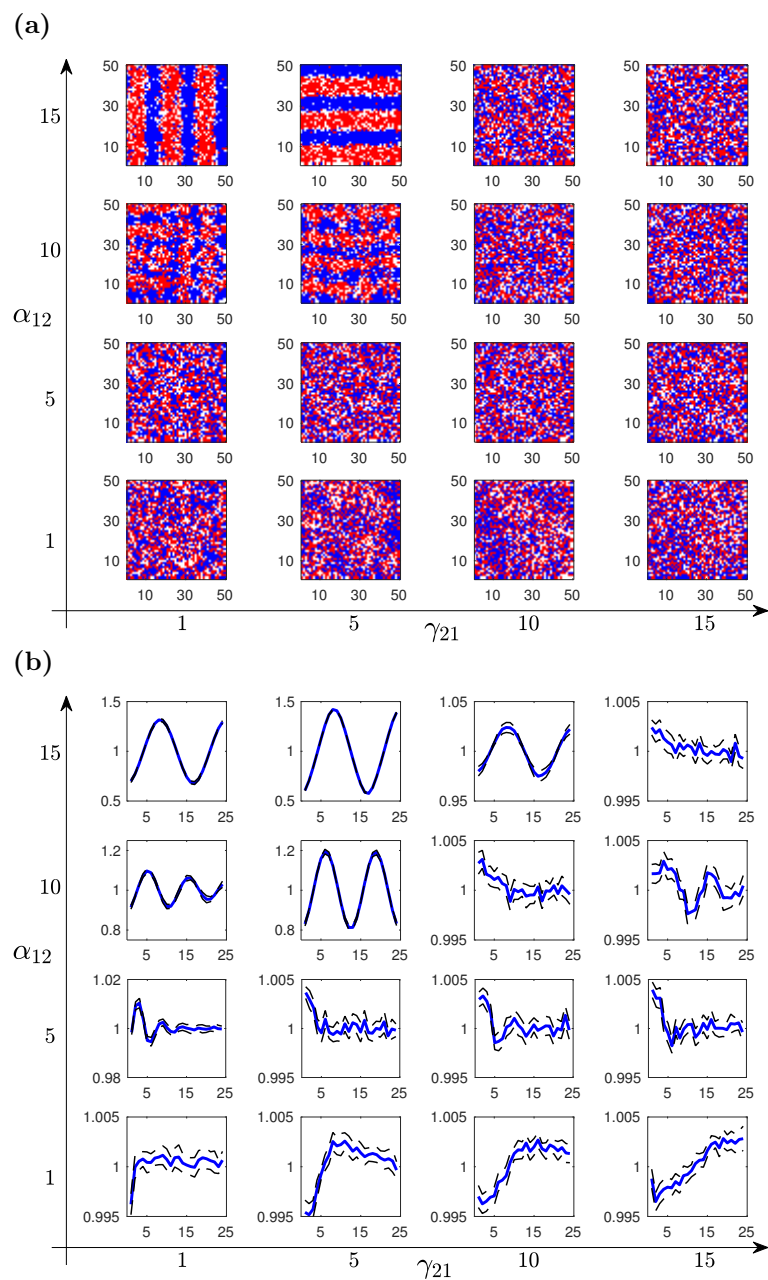
Figure 9: Attractive-repulsive interactions with no homotypic interactions, $a_{12} = r_{21} = 1$, $a_{21} = r_{12} = 0$, $a_{11} = a_{22} = r_{11} = r_{22} = 0$, and $N_1 = N_2 = 1000$. The effect of varying the heterotypic ranges attraction / repulsion is shown, $\alpha_{21} = \gamma_{21} = \{1, 5, 10, 15\}$. (a) Typical spatial patterns. (b) Average heterotypic PCF, g_{12}.
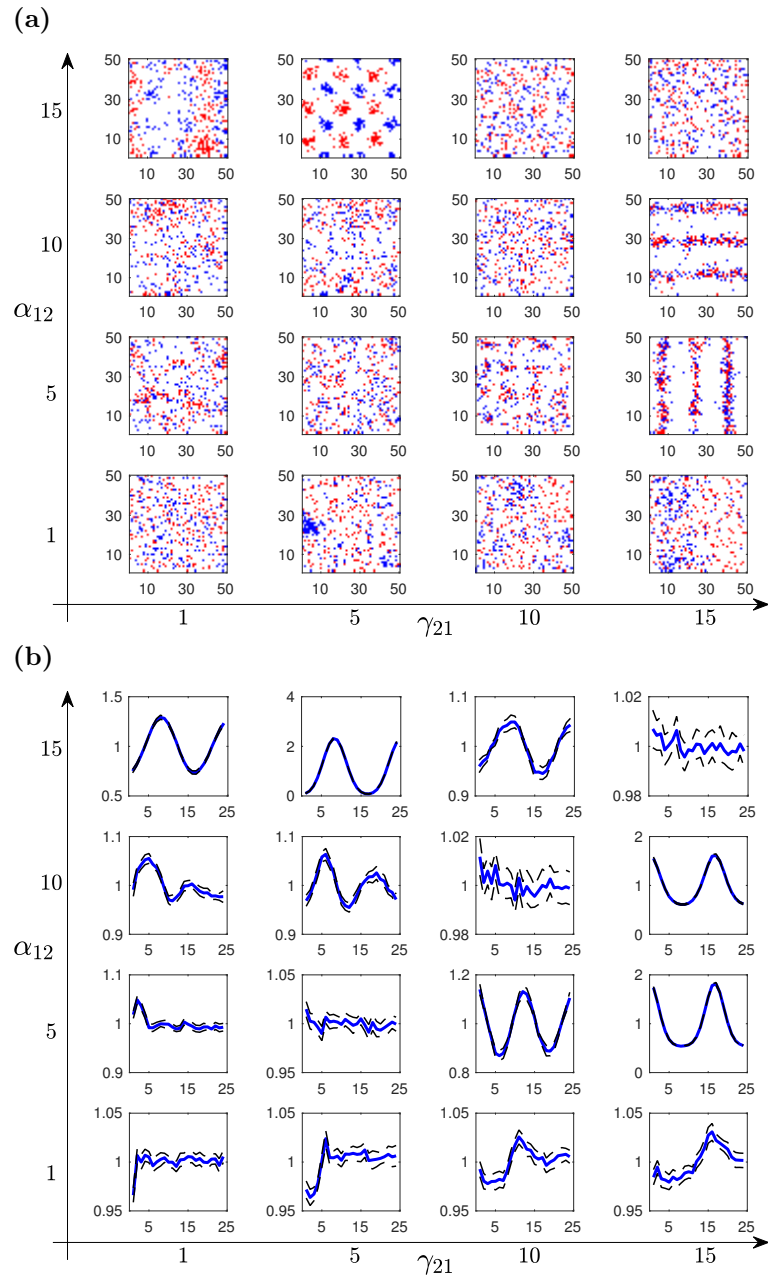
Figure 10: Attractive-repulsive interactions with no homotypic interactions, $a_{12} = r_{21} = 1$, $a_{21} = r_{12} = 0$, $a_{11} = a_{22} = r_{11} = r_{22} = 0$, and $N_1 = N_2 = 200$. The effect of varying the heterotypic ranges attraction / repulsion is shown, $\alpha_{21} = \gamma_{21} = \{1, 5, 10, 15\}$. (a) Typical spatial patterns. (b) Average heterotypic PCF, g_{12}.

19

and maintenance of the stripes. Woolley *et al.* (2014) posits a similar argument that run-and-chase does not lead to formation of persistent stripes, using a lattice-free individual-based model. The results presented in Fig. 9 confirm that when the heterotypic interactions have equal ranges, stripe formation does not occur. However, if the range of attraction is longer than that of repulsion, stripes can be produced without the need for homotypic interactions.

Finally, we examine the effect of reducing the densities by one fifth in the run-and-chase simulations of Fig. 9. The importance of density on pattern formation is demonstrated by comparing the panels in Figs. 9 and 10, where we can observe that the intra-species stripes in the high density system are not present in the lower density system. Furthermore, the lower density simulations produce a new type of pattern of interspecies stripes separated by stripes of unoccupied space within the domain (see the fourth column, Fig. 10). Therefore, it is possible that other families of patterns, such as the ring-like structures observed in the single species models of Liu *et al.* (2013) and Martínez-García *et al.* (2015), could be found by further exploration of the parameter space with our multi-species model.

4 Discussion

In this paper, we have developed a generic ABM for two interacting species. The interactions between individuals can be attractive or repulsive in any combination, and the ranges of interactions can be varied for each type of interaction. The model enables us to investigate how different inter-individual interactions can generate a variety of distinctive, large-scale patterns. However, the main novelty of our approach is to combine the agent-based modelling with a method of quantifying the resulting patterns, which provides a means by which model results and experimental observations can be compared, and the underlying inter-individual interactions identified. We have extended the periodic PCF introduced in [1] to allow us to quantify the multi-species spatial patterns produced by different combinations of homotypic and heterotypic interactions, and have shown how to interpret the PCF and obtain information about the underlying interactions.

We began by considering the case where the heterotypic interactions between the two species were either both attractive or both repulsive. For the case of strong heterotypic attraction (in the absence of homotypic interactions), compact aggregates form in which both types of individuals are intermixed, which is consistent with the results of [19], who considered interactions between two types of liver cell cultured *in vitro*. Conversely, when homotypic attraction dominates over heterotypic, compact aggregates form in which the two types are segregated. Interestingly, and perhaps less intuitively, we observe the formation of similar compact, segregated aggregates when the dominant interaction is heterotypic repulsion, combined with weaker homotypic attraction. This is because the strong repulsion 'sorts' the agents into regions where only one type is present, and the weak homotypic attraction then causes them to coalesce into clumps. Although both situations give rise to aggregates of the same composition, the difference in the interactions can be distinguished by our PCF. Similar to the results of Agnew *et al.* (2014), our PCF is also able to identify weak interactions, even if the resulting pattern is indistinguishable by eye from the CSR state. However, in general, interpretation of the two-species PCFs is more complicated than for the one-species case; for example, the fact that the function is greater than unity does not necessarily indicate an attractive interaction (see *e.g.*, Fig. 5). These results emphasise the importance of both quantification, and careful experimentation to explore all the possibilities when investigating interactions in biological systems.

We then turned our attention to the case of attractive-repulsive heterotypic interactions - the

run-and-chase scenario. We considered two biological examples of this situation: predator-prey interactions, and melanophore-xanthophore interactions in zebrafish. In the first of these, we were able to demonstrate using the PCF that increasing the strength of homotypic attraction between the prey would lead to closer proximity of predators and prey on average, which would be to the advantage of the predators. We believe this is due to the fact that the homotypic attractions help to maintain a compact, coherent group of prey, which is more strongly attractive to the predators than a more dispersed group would be. Similar to some of the earlier cases, this result is not obvious from visual comparison of the patterns (see Fig. 8), and so provides another example of the potential usefulness of the PCF in quantifying the spatial distributions of individuals.

Run-and-chase has also been proposed as the mechanism giving rise to stripe formation in zebrafish [61, 23], and we investigated this possibility using our model. We varied the ranges of attraction (xanthophores towards melanophores) and repulsion (melanophores towards xanthophores) to determine which values would lead to the initiation of stripes. Long range attraction and short range repulsion was found to be able to produce stripes. Importantly, we found that homotypic attraction is not necessary for stripe formation, in contrast to what has been suggested by Painter *et al.* (2015) and Woolley *et al.* (2014).

The ABM used here is an idealised, simple model, intended to cover a wide range of situations driven by homotypic-heterotypic attraction-repulsion forces. One can specialise this model for a specific system by including more underlying mechanisms. Some examples include incorporating lattice growth to mimic the growth in the size of the zebrafish during its development [58], or adding mechanisms, such as predator confusion [27], active defending [28], *etc.* to the predator-prey model to gain insight into how different swarming behaviours may be advantageous in these species.

Our PCF may also be useful for the purpose of parameter estimation. Recent work on parameter inference for simpler (one population) ABMs suggest that it is a good candidate for use as a summary statistic in approximate Bayesian computation methods [54, 25, 51]. However, we note that due to the higher complexity of our model (which includes attraction and repulsion strengths and lengthscales for each combination of interactions), extending the previous work will be a considerable undertaking.

Acknowledgements

References

[1] D. J. G. Agnew, J. E. F. Green, T. M. Brown, M. J. Simpson, and B. J. Binder. Distinguishing between mechanisms of cell aggregation using pair-correlation functions. *Journal of Theoretical Biology*, 352:16–23, jul 2014. ISSN 10958541. doi: 10.1016/j.jtbi.2014.02.033.

[2] L. Angelani. Collective Predation and Escape Strategies. *Physical Review Letters*, 109(11): 118104, sep 2012. ISSN 0031-9007. doi: 10.1103/PhysRevLett.109.118104.

[3] P. Ball. Pattern formation in nature: Physical constraints and self-organising characteristics. *Architectural Design*, 82(2):22–27, 2012. ISSN 00038504. doi: 10.1002/ad.1375.

[4] B. J. Binder and K. A. Landman. Exclusion processes on a growing domain. *Journal of Theoretical Biology*, 259(3):541–551, 2009. ISSN 00225193. doi: 10.1016/j.jtbi.2009.04.025.

[5] B. J. Binder and M. J. Simpson. Quantifying spatial structure in experimental observations and agent-based simulations using pair-correlation functions. *Physical Review E - Statistical, Nonlinear, and Soft Matter Physics*, 88(2):22705, 2013. ISSN 15393755. doi: 10.1103/PhysRevE.88.022705.

[6] B. J. Binder, J. F. Sundstrom, J. M. Gardner, V. Jiranek, and S. G. Oliver. Quantifying Two-Dimensional Filamentous and Invasive Growth Spatial Patterns in Yeast Colonies. *PLoS Computational Biology*, 11(2):e1004070—-e1004070, 2015. ISSN 15537358. doi: 10. 1371/journal.pcbi.1004070.

[7] D. Bullara and Y. De Decker. Pigment cell movement is not required for generation of Turing patterns in zebrafish skin. *Nature communications*, 6(May):6971, 2015. ISSN 2041-1723. doi: 10.1038/ncomms7971.

[8] A. Cazaubiel, A. F. Lütz, and J. J. Arenzon. Collective strategies and cyclic dominance in asymmetric predator-prey spatial games. *Journal of Theoretical Biology*, 430:45–52, oct 2017. ISSN 10958541. doi: 10.1016/j.jtbi.2017.07.002.

[9] Y. Chen and T. Kolokolnikov. A minimal model of predator-swarm dynamics. *Journal of the Royal Society Interface*, I(1):20131208, 2014. ISSN 1742-5689. doi: 10.1098/rsif.2013. 1208.

[10] I. D. Couzin, J. Krause, R. James, G. D. Ruxton, and N. R. Franks. Collective memory and spatial sorting in animal groups. *Journal of Theoretical Biology*, 218(1):1–11, 2002. ISSN 00225193. doi: 10.1006/yjtbi.3065.

[11] S. C. Cowin. How Is a Tissue Built? *Journal of Biomechanical Engineering*, 122(6):553, jul 2000. ISSN 0148-0731. doi: 10.1115/1.1324665.

[12] X. Cui, S. Dini, S. Dai, J. Bi, B. J. Binder, J. E. F. Green, and H. Zhang. A mechanistic study on tumour spheroid formation in thermosensitive hydrogels: experiments and mathematical modelling. *RSC Adv.*, 6(77):73282–73291, 2016. ISSN 2046-2069. doi: 10.1039/C6RA11699J.

[13] P. J. Diggle. *Statistical Analysis of Spatial Point Patterns*. Academic Press, 2003.

[14] S. Dini, B. J. Binder, S. C. Fischer, C. Mattheyer, A. Schmitz, E. H. K. Stelzer, N. G. Bean, and J. E. F. Green. Identifying the necrotic zone boundary in tumour spheroids with pair-correlation functions. *Journal of The Royal Society Interface*, 13(123):1–20, 2016. ISSN 1742-5662. doi: http://dx.doi.org/10.1098/rsif.2016.0649.

[15] R. C. Fetecau, Y. Huang, and T. Kolokolnikov. Swarm dynamics and equilibria for a nonlocal aggregation model. *Nonlinearity*, 24(10):2681–2716, 2011. ISSN 09517715 13616544. doi: 10.1088/0951-7715/24/10/002.

[16] J. A. Fozard, G. R. Kirkham, L. D. Buttery, J. R. King, O. E. Jensen, and H. M. Byrne. Techniques for analysing pattern formation in populations of stem cells and their progeny. *BMC bioinformatics*, 12(1):396, 2011. ISSN 1471-2105. doi: 10.1186/1471-2105-12-396.

[17] H. G. Frohnhöfer, J. Krauss, H.-M. Maischein, and C. Nüsslein-Volhard. Iridophores and their interactions with other chromatophores are required for stripe formation in zebrafish. *Development (Cambridge, England)*, 140(14):2997–3007, 2013. ISSN 1477-9129. doi: 10.1242/dev.096719.

[18] E. A. Gaffney and S. Seirin Lee. The sensitivity of turing self-organization to biological feedback delays: 2D models of fish pigmentation. *Mathematical Medicine and Biology*, 32 (1):56–78, 2015. ISSN 14778602. doi: 10.1093/imammb/dqt017.

[19] J. E. F. Green, S. L. Waters, J. P. Whiteley, L. Edelstein-Keshet, K. M. Shakesheff, and H. M. Byrne. Non-local models for the formation of hepatocyte-stellate cell aggregates. *Journal of Theoretical Biology*, 267(1):106–120, 2010. ISSN 00225193. doi: 10.1016/j.jtbi.2010.08.013.

[20] E. J. Hackett-Jones, K. A. Landman, and K. Fellner. Aggregation patterns from nonlocal interactions: Discrete stochastic and continuum modeling. *Physical Review E - Statistical, Nonlinear, and Soft Matter Physics*, 85(4):41912, 2012. ISSN 15393755. doi: 10.1103/PhysRevE.85.041912.

[21] H. Hamada, M. Watanabe, H. E. Lau, T. Nishida, T. Hasegawa, D. M. Parichy, and S. Kondo. Involvement of Delta/Notch signaling in zebrafish adult pigment stripe patterning. *Development (Cambridge, England)*, 141(2):318–24, 2014. ISSN 1477-9129. doi: 10.1242/dev.099804.

[22] D. J. Illian, P. A. Penttinen, D. D. H. Stoyan, D. D. H. Stoyan, and J. Illian. *Statistical Analysis and Modelling of Spatial Point Patterns*, volume 76. John Wiley & Sons, 2008. ISBN 9780470014912. doi: 10.1111/j.1751-5823.2008.00062_23.x.

[23] M. Inaba, H. Yamanaka, and S. Kondo. Pigment pattern formation by contact-dependent depolarization. *Science*, 335(6069):677, 2012.

[24] S. Inoue, S. Kondo, D. M. Parichy, and M. Watanabe. Tetraspanin 3c requirement for pigment cell interactions and boundary formation in zebrafish adult pigment stripes. *Pigment Cell and Melanoma Research*, 27(2):190–200, 2014. ISSN 17551471. doi: 10.1111/pcmr.12192.

[25] S. T. Johnston, M. J. Simpson, D. L. S. McElwain, B. J. Binder, and J. V. Ross. Interpreting scratch assays using pair density dynamics and approximate Bayesian computation. *Open biology*, 4(9):140097, 2014. ISSN 2046-2441. doi: 10.1098/rsob.140097.

[26] E. F. Keller and L. A. Segel. Initiation of slime mold aggregation viewed as an instability. *Journal of Theoretical Biology*, 26(3):399–415, 1970. ISSN 10958541. doi: 10.1016/0022-5193(70)90092-5.

[27] D. C. Krakauer. Groups confuse predators by exploiting perceptual bottlenecks: a connectionist model of the confusion effect. *Behavioral Ecology and Sociobiology*, 36(6):421–429, jun 1995. ISSN 0340-5443. doi: 10.1007/BF00177338.

[28] J. Krause and G. D. Ruxton. *Living in groups*. Oxford University Press, 2002.

[29] C. Lett, P. Auger, and J. M. Gaillard. Continuous cycling of grouped vs. solitary strategy frequencies in a predator-prey model. *Theoretical Population Biology*, 65(3):263–270, may 2004. ISSN 00405809. doi: 10.1016/j.tpb.2003.10.005.

[30] Q.-X. Liu, A. Doelman, V. Rottschäfer, M. de Jager, P. M. J. Herman, M. Rietkerk, and J. van de Koppel. Phase separation explains a new class of self-organized spatial patterns in ecological systems. *Proceedings of the National Academy of Sciences of the United States of America*, 110(29):11905–10, jul 2013. ISSN 1091-6490. doi: 10.1073/pnas.1222339110.

[31] M. Luca, A. Chavez-Ross, L. Edelstein-Keshet, and A. Mogilner. Chemotactic signaling, microglia, and Alzheimer's disease senile plaques: Is there a connection? *Bulletin of Mathematical Biology*, 65(4):693–730, 2003. ISSN 00928240. doi: 10.1016/S0092-8240(03)00030-2.

[32] A. F. Lütz, S. Risau-Gusman, and J. J. Arenzon. Intransitivity and coexistence in four species cyclic games. *Journal of Theoretical Biology*, 317:286–292, 2013. ISSN 00225193. doi: 10.1016/j.jtbi.2012.10.024.

[33] R. Martínez-García, C. Murgui, E. Hernández-García, C. López, P. Herman, and M. Rietkerk. Pattern Formation in Populations with Density-Dependent Movement and Two Interaction Scales. *PLOS ONE*, 10(7):e0132261, jul 2015. ISSN 1932-6203. doi: 10.1371/journal.pone.0132261.

[34] S. K. McMenamin, E. J. Bain, A. E. McCann, L. B. Patterson, D. S. Eom, Z. P. Waller, J. C. Hamill, J. A. Kuhlman, J. S. Eisen, and D. M. Parichy. Thyroid hormone–dependent adult pigment cell lineage and pattern in zebrafish. *Science*, 345(6202):1358–1361, 2014.

[35] A. M. Middleton, C. Fleck, and R. Grima. A continuum approximation to an off-lattice individual-cell based model of cell migration and adhesion. *Journal of Theoretical Biology*, 359:220–232, 2014. ISSN 10958541. doi: 10.1016/j.jtbi.2014.06.011.

[36] A. Mogilner and L. Edelstein-Keshet. A non-local model for a swarm. *Journal of Mathematical Biology*, 38(6):534–570, 1999.

[37] A. Mogilner, L. Edelstein-Keshet, L. Bent, and A. Spiros. Mutual interactions, potentials, and individual distance in a social aggregation. *Journal of Mathematical Biology*, 47(4):353–389, 2003. ISSN 03036812. doi: 10.1007/s00285-003-0209-7.

[38] J. Moreira and A. Deutsch. Pigment pattern formation in zebrafish during late larval stages: A model based on local interactions. *Developmental Dynamics*, 232(1):33–42, 2005. ISSN 10588388. doi: 10.1002/dvdy.20199.

[39] L. J. Morrell, G. D. Ruxton, and R. James. Spatial positioning in the selfish herd. *Behavioral Ecology*, 22(1):16–22, jan 2011. ISSN 1045-2249. doi: 10.1093/beheco/arq157.

[40] R. L. Mort, R. J. H. Ross, K. J. Hainey, O. J. Harrison, M. A. Keighren, G. Landini, R. E. Baker, K. J. Painter, I. J. Jackson, and C. A. Yates. Reconciling diverse mammalian pigmentation patterns with a fundamental mathematical model. *Nature Communications*, 7:10288, jan 2016.

[41] T. L. Morton, J. W. Haefner, V. Nugala, R. D. Decino, and L. Mendes. The Selfish Herd Revisited: Do Simple Movement Rules Reduce Relative Predation Risk? *Journal of Theoretical Biology*, 167(1):73–79, mar 1994. ISSN 00225193. doi: 10.1006/jtbi.1994.1051.

[42] J. Murray. A Pre-pattern formation mechanism for animal coat markings. *Journal of Theoretical Biology*, 88(1):161–199, jan 1981. ISSN 00225193. doi: 10.1016/0022-5193(81)90334-9.

[43] J. D. Murray. A Pattern Formation Mechanism and Its Application to Mammalian Coat Markings. pages 360–399. Springer, Berlin, Heidelberg, 1980. doi: 10.1007/978-3-642-93161-1_20.

[44] J. D. Murray. On Pattern Formation Mechanisms for Lepidopteran Wing Patterns and Mammalian Coat Markings. *Philosophical Transactions of the Royal Society of London B: Biological Sciences*, 295(1078), 1981.

[45] A. Nakamasu, G. Takahashi, A. Kanbe, and S. Kondo. Interactions between zebrafish pigment cells responsible for the generation of Turing patterns. *Proceedings of the National Academy of Sciences of the United States of America*, 106(21):8429–34, 2009. ISSN 1091-6490. doi: 10.1073/pnas.0808622106.

[46] R. Olfati-Saber. Flocking for Multi-Agent Dynamic Systems:Algorithms and Theory. *IEEE Transactions on Automatic Control*, 51(3):1–20, 2006. ISSN 00189286. doi: 10.1109/TAC.2005.864190.

[47] R. S. Olson, D. B. Knoester, and C. Adami. Evolution of Swarming Behavior Is Shaped by How Predators Attack. *Artificial Life*, 22(3):299–318, aug 2016. ISSN 1064-5462. doi: 10.1162/ARTL_a_00206.

[48] K. J. Painter, J. M. Bloomfield, J. A. Sherratt, and A. Gerisch. A Nonlocal Model for Contact Attraction and Repulsion in Heterogeneous Cell Populations. *Bulletin of Mathematical Biology*, 77(6):1132–1165, 2015. ISSN 0092-8240. doi: 10.1007/s11538-015-0080-x.

[49] J. K. Parrish and L. Edelstein-Keshet. Complexity, pattern, and evolutionary trade-offs in animal aggregation. *Science*, 284(5411):99–101, 1999.

[50] L. B. Patterson, E. J. Bain, D. M. Parichy, C. Nüsslein-Volhard, and D. M. Parichy. Pigment cell interactions and differential xanthophore recruitment underlying zebrafish stripe reiteration and Danio pattern evolution. *Nature Communications*, 5:5299, nov 2014. ISSN 2041-1723. doi: 10.1038/ncomms6299.

[51] R. J. H. Ross, R. E. Baker, A. Parker, M. J. Ford, R. L. Mort, and C. A. Yates. Using approximate Bayesian computation to quantify cellcell adhesion parameters in a cell migratory process. *npj Systems Biology and Applications*, 3(1):9, 2017. ISSN 2056-7189. doi: 10.1038/s41540-017-0010-7.

[52] M. J. Simpson, K. A. Landman, and B. D. Hughes. Multi-species simple exclusion processes. *Physica A: Statistical Mechanics and its Applications*, 388(4):399–406, 2009. ISSN 03784371. doi: 10.1016/j.physa.2008.10.038.

[53] R. J. Thomas, A. Bennett, B. Thomson, and K. M. Shakesheff. Hepatic stellate cells on poly(DL-lactic acid) surfaces control the formation of 3D hepatocyte co-culture aggregates in vitro. *European Cells and Materials*, 11:16–26, 2006. ISSN 14732262. doi: vol011a03[pii].

[54] T. Toni, D. Welch, N. Strelkowa, A. Ipsen, M. P. Stumpf, and C. A. Yates. Approximate Bayesian computation scheme for parameter inference and model selection in dynamical systems. *Journal of The Royal Society Interface*, 6(31):187–202, feb 2009. ISSN 1742-5689. doi: 10.1098/rsif.2008.0172.

[55] C. M. Topaz, A. J. Bernoff, S. Logan, and W. Toolson. A model for rolling swarms of locusts. In *European Physical Journal: Special Topics*, volume 157, pages 93–109, 2008. ISBN 1951-6355. doi: 10.1140/epjst/e2008-00633-y.

[56] K. K. Treloar, M. J. Simpson, B. J. Binder, D. L. S. McElwain, and R. E. Baker. Assessing the role of spatial correlations during collective cell spreading. *Scientific reports*, 4:5713, 2014. ISSN 2045-2322. doi: 10.1038/srep05713.

[57] A. M. Turing. The chemical basis of morphogenesis. *Philosophical Transactions of the Royal Society of London B: Biological Sciences*, 237(641):37–72, 1952.

[58] A. Volkening and B. Sandstede. Modelling stripe formation in zebrafish: an agent-based approach. *Journal of The Royal Society Interface*, 12(112):20150812, nov 2015. ISSN 1742-5689, 1742-5662. doi: 10.1098/rsif.2015.0812.

[59] T. E. Woolley, P. K. Maini, and E. A. Gaffney. Is pigment cell pattern formation in zebrafish a game of cops and robbers? *Pigment Cell & Melanoma Research*, 27(5):686–687, sep 2014. ISSN 17551471. doi: 10.1111/pcmr.12276.

[60] M. Yamaguchi, E. Yoshimoto, and S. Kondo. Pattern regulation in the stripe of zebrafish suggests an underlying dynamic and autonomous mechanism. *Proceedings of the National Academy of Sciences*, 104(12):4790–4793, mar 2007. ISSN 0027-8424, 1091-6490. doi: 10.1073/pnas.0607790104.

[61] H. Yamanaka and S. Kondo. In vitro analysis suggests that difference in cell movement during direct interaction can generate various pigment patterns in vivo. *Proceedings of the National Academy of Sciences*, 111(5):1867–1872, feb 2014. ISSN 0027-8424, 1091-6490. doi: 10.1073/pnas.1315416111.

[62] V. Zhdankin and J. C. Sprott. Simple predator-prey swarming model. *Physical Review E*, 82(5):056209, nov 2010. ISSN 1539-3755. doi: 10.1103/PhysRevE.82.056209.